

Design for Additive Manufacturing: Multi Material Sand Mold

T. A. Le Néel^{1, a}, P. Mognol^{2, b}, J. Y. Hascoët^{1, c}

¹ Centrale Nantes, 1 rue de la Noë, Nantes 44321 cedex 3, France UMR CNRS 6183

² École Normale Supérieure de Rennes, Avenue Robert Schuman, 35170 Bruz, France UMR CNRS 6183

^atugdual.le-neel@ec-nantes.fr, ^bpascal.mognol@ens-rennes.fr, ^cjean-yves.hascoet@ec-nantes.fr

Abstract

Indirect additive manufacturing is an alternative way to produce metal parts by using foundry practices. This paper will detail a novel method that uses the additive manufacturing process of binder jetting with different powders such as silica, aluminum, alumina, and steel to create a multi material mold. Multi material 3D printed molds and cores can improve parts' design freedom, this methodology gives the ability to have a specific thermal conductivity at a specific location in order to remove or displace hot spots. The reduction of hot spots enables geometries that are more complex and are said to be impossible via traditional sand casting.

A binder jetting 3D printer was developed to additively manufacture molds and core with an inorganic binder. Simulation softwares indicate material's properties and design pertinence.

Keywords: Additive Manufacturing, Casting, DFAM, Sand Mold, Optimization

1. Introduction

Many jobs will change with the 4.0 industry as in the digital age, manual labor is reduced to make room for automation. Nowadays, sand casting still requires modelers to design and fabricate the patterns to make the molds. Those patterns are usually milled from wood blanks. The pattern is then pressed down onto sand by hand to leave an imprint. Once the pattern is removed, the multiple parts of the mold can be assembled. Finally, the founder adds sprue, runner, and the multiples risers before pouring metal in the mold as detailed in figure 1. All those laborious tasks can be simplified with additive manufacturing (AM) the art of layer a material on top of another. In this case, binder is jetted out of multiple nozzles at a select location during a certain amount of time onto a granular material in order to make a 3D part. Laser sintering is another AM technique for manufacturing parts from a granular base material that could work with the proposed methodology [1] [2].

Usually, AM is for direct manufacturing, therefore some have explored the possibilities of binder jetting metal powder for as a final product [3] [4] [5]. Indirect additive manufacturing (IAM) is the technique of fabrication molds and cores by additive manufacturing. In this case, the molds and cores are not the final product but a tool to fabricate desired parts. Indirect additive manufacturing can be, a positive model which is then covered with ceramic [9] [10], or a direct printing the mold [11].

One of the advantages of IAM is if the mold is made in one piece. The problem of mismatching the plates is removed, which leads to higher quality part. It also reduces turn around time as mold manipulation is reduced and pattern fabrication is inexistent. Draft angles can be negative as no pattern is required. AM can help in resolving thermal management problems, such as misruns, cold shuts, microporosity. Another advantage of IAM is the fabrication of varying thickness sand shells molds and cores as to manage ideal thickness [12]. Furthermore, if we exploit the selective placement of materials, the quantity of binder can be adjusted as to vary the thermal and mechanical properties. The current methodology is for multi material which are not blended like other work in which they are functionally graded materials [13].

Design for Additive Manufacturing (DFAM) will ease the adoption of AM as it will enhance the technology. Indeed, if a part is design for the process, the more can be done with less. DFAM has been proposed for other processes like LMD [6] or Polyjet [7]. Additive manufacturing with no DFAM has already impacted the casting industry at multiple such as : wax pattern / pattern, shell moulding / moulding, and cores boxes [8].

This study goes over the impact of placing specific materials at a specific location for their thermal properties. Numerical simulations casting indicate that placing the right material at the right place in the right quantity can improve the geometrical and mechanical properties of the final metal casting. This methodology relies on the 3D printer's on the capabilities to handle multiple materials during the same build job. Yet, this feature is limited to a few commercialized machines and research projects.

The 3D printer developed is based on a Stäubli TX90 6-axis robotic arm equipped with multiple HP C6602 cartridges.

Figure 2 illustrates the binder jetting principle when using a robot. The tool is comprised of the binder jetting tool, a doctor blade, and the sand hopper. The resolution of the print head is 96 dpi. Those cartridges were emptied and modified to be compatible with sodium silicate inorganic binder 3D printing. Inorganic binder has the advantage of not releasing any CO₂ during the casting process. Carbon dioxide is usually released during the degradation of the organic binder (carbon based) when it combines with ambient oxygen. Once printed, the mold is in a green state a curing step is necessary. The inorganic 3D printed molds undergo a curing stage in an oven at 110 °C for 120 min. Usually, the curing is done in a microwave at 700 W for 120 seconds, but the metallic particles prohibit the use of this tool. Microwave heating drastically quickens the process. The multi material mold is an assembly of multiple prints in this case as multi material fabrication is not possible with this set up.

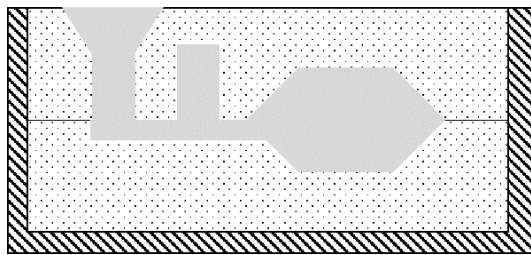


Figure 1 Sand Casting

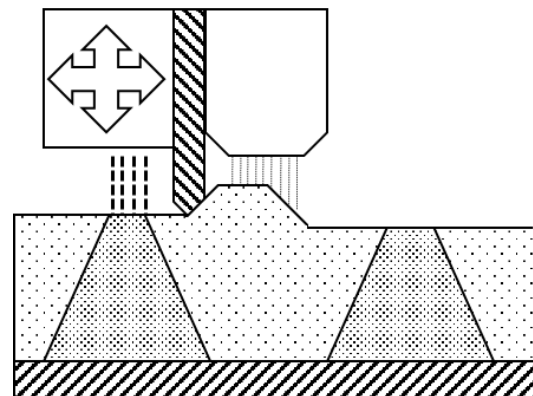


Figure 2 3D Printing technique

2. Mold Characterization

2.1. Thermal Conductivity

Thermal characterization of the 3D printed sand mold is acquired in order to have real world input data for the numerical simulation. Silica sand used in casting is used, granulometry of 120 μm with some grains being twice as big and some twice as small and is fairly angular with an aspect ratio of roughly 0.1 x 0.1 [14]. The silica sand used, figure 3, has a high probability of being crush silica sand. Aluminum and steel powder used for AM LMD process is used. Aluminum powder has a diameter size of around 40 μm and is fairly round. Steel powder has a granulometry of 45 μm – 90 μm and was very spherical with an aspect ratio of 0.9 x 0.9, figure 4. Alumina powder's diameter was between 2 μm and 5 μm.

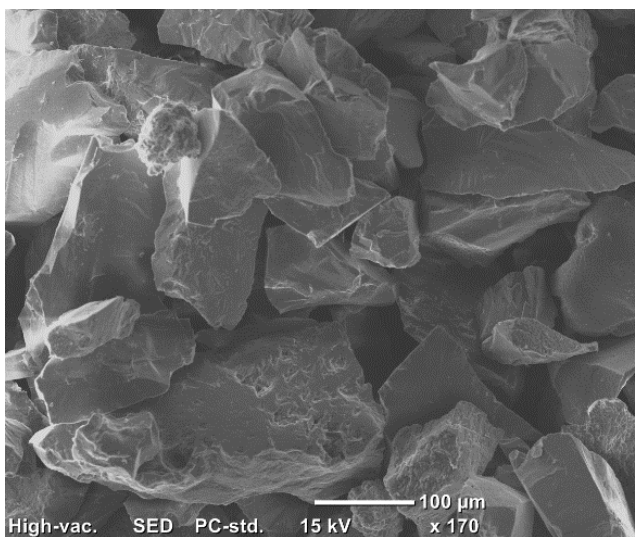


Figure 3 MEB silica sand

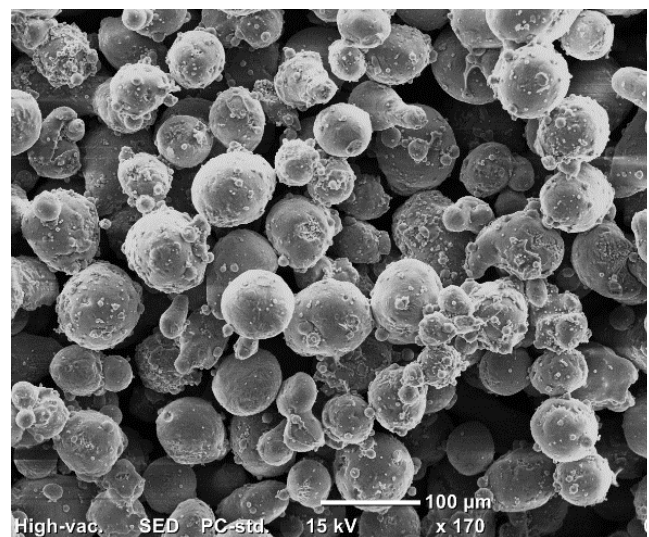


Figure 4 MEB aluminum powder

The conductivity of granular material is not evident as it depends on the sphericity, particle diameter, and pressure [15].

Thermal conductivity analysis was obtained with a Linseis THB 100 machine. The analysis relies on the principle of a self

heated wire. The sensor used is for Quasi-Steady-State (QSS) which is able to measure a 0.1 W/(m·K) to 200 W/(m·K). A constant heat flow provided by a constant power to the resistor is applied, the measured temperature rise can infer the thermal conductivity of the material. Prepared sample size was of 40 mm x 50 mm x 4 mm. Then “Hand built” were molded by hand with regular tooling, and the “3D printed” were printed with the robot. All samples testing were at ambient temperature between 23 °C and 24 °C the same day. Table 1 recapitulates the results.

Material	Thermal Conductivity (W/(m·K))	
	Hand built	3D printed
Silica sand (120 μm)	0.6	0.4
Silica sand (1 200 μm)	-	-
316L	1.2	0.6
Alumina	0.4	-
Aluminum	1.2	1.0

Table 1 Thermal conductivity results

3D printing of alumina powder was not possible as it was too volatile. There is a decrease in thermal conductivity from “hand built” to “3D printed” as the density is lower. Indeed, during 3D printing the sand is dropped onto the previous layer. The doctor blade used to rack the sand does not compress the layers. This phenomenon creates voids within the structure, hence making it less conductive. It was hypothesize that aluminum powder would be much more conductive as the base material is a good conductor, but results show otherwise. It is believed this is due to the process and binder choice. The higher diameter silica sand was not testable with this method as too much void was present between the grains.

Figure 5 illustrates the different configurations of the powder. “Theoretical no binder” configuration (a) should yield a thermal conductivity value close the theoretical thermal conductivity of bulk material. But this configuration does not represent well enough the process, binder has to be added. If little binder is added then we are in configuration b) and if too much binder is added then in configuration c). Those configurations may suggest that the thermal conductivity is a combination of bulk material and binder thermal conductivities, closer to reality. Yet, when MEB analysis is performed on the granular structure, lots of void is present. The binder jetting process is better modeled with configuration d), in which the particles are not touching and thermal conductivity is mainly dictated by the binder’s properties. Furthermore, the shape of the particles is not as spherical as depicted, which will impact the thermal properties.

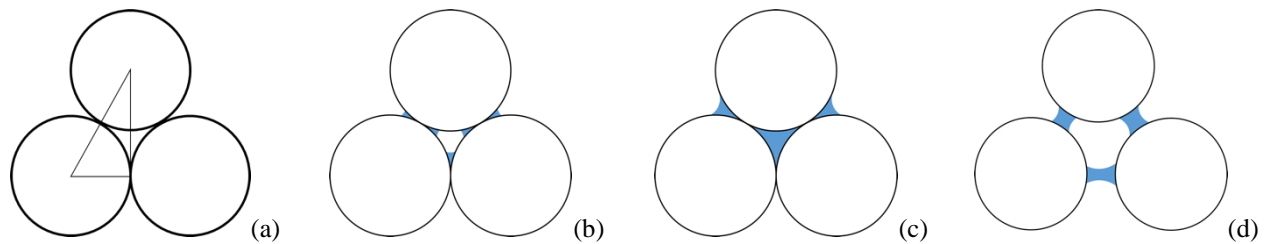


Figure 5 Powder arrangement during binder jetting process a) theoretical no binder, b) with binder, c) binder saturation, d) actual

The thermal conductivity does not change as much as predicted but other factors may come into play. The thermal interface coefficient should vary when changing the base material. The radiation coefficient and the wetting capability is not the same. Casting with thermocouples at different distances should indicate better realistic values.

2.2 Powder’s Influence on Compression Strength

Samples size of 10 mm x 10 mm x 10 mm have been additively fabricated. The samples were slightly sanded down to roughly 7 mm x 7 mm x 7 mm as to remove any residual stratification from the process. All samples were not exactly of the same dimensions. The compression press’s upper die had a 5 mm diameter. Maximum load until rupture is recorded. Binder ratio is about 9 % in weight with silica sand (120 μm) as a reference. The results are presented in table 2.

Material	Compression strength (MPa)
Silica sand (120 μm)	1.5
Silica sand (1 200 μm)	0.6
Aluminum	3
Steel	1.2

Table 2 Compression tests results

The quantity of binder deposited is the same for every sample, but the binder ratio is not the same for all samples. This discrepancy is due to the powder's varying diameter and density.

3. Design Guidelines & Numerical Methods

Design for sand casting rules prohibit multiple geometries such as sharp corners, figure 6 to prevent hot spots or other casting defects, figure 7 [16],[17]. To reduce the shrink defect induced by hot spots, rounded corners (fillets or radii) are introduced.

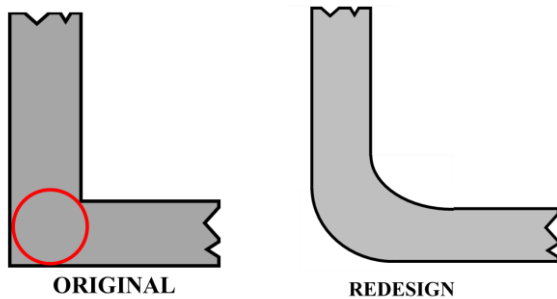


Figure 6 Sharp angle geometry guideline [16]

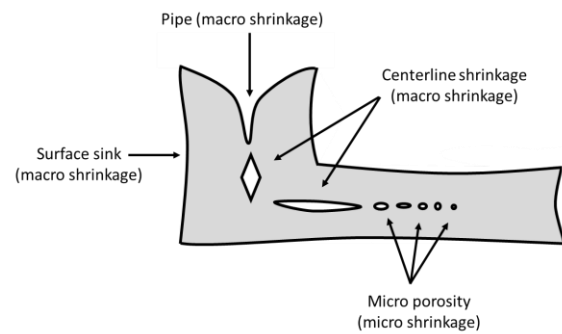


Figure 7 Sources of defects [17]

The addition of fillets helps even the cooling speed as described by Niyama [17]. The Niyama criterion eq. 1 is used to be sure the thermal gradient is not hindering the quality of the casted part.

$$N = \frac{G}{\sqrt{R_c}} \quad (1)$$

R_c is the cooling speed expressed in K/s and G the thermal gradient expressed in K/cm. Lower the value is, more likely will the casting be sound. In our case study, we are setting the limit for aluminum at $0.3 \text{ (K}\cdot\text{s)}^{-1/2}\cdot\text{cm}^{-1}$ [18].

A 2D approach via COMSOL Metaphysics is first exploited as a proof of concept for dual material sand molds. The simulation represents an aluminum cube heated at $700 \text{ }^\circ\text{C}$ and the cooled at ambient temperature of $20 \text{ }^\circ\text{C}$. The cube is cut alongside of its symmetry's planes to reduce calculation time. The baseline mold's properties are equivocal of silica sand, while the other material properties are those of estimated aluminum powder properties. The aluminum powder is chosen for its higher thermal conductivity at $10 \text{ W}/(\text{m}\cdot\text{K})$ and alumina for slower conductivity at $0.1 \text{ W}/(\text{m}\cdot\text{K})$. Further settings include a thermal capacity of $700 \text{ J}/(\text{kg}\cdot\text{K})$, a density of $2329 \text{ kg}/\text{m}^3$ and an interface coefficient h of $1 \text{ MW}/(\text{m}^2\cdot\text{K})$, although those values may change between aluminum and alumina, in this case they are kept the same. The metal solidus is at $548 \text{ }^\circ\text{C}$ and liquidus of $613 \text{ }^\circ\text{C}$, the latent heat is $431 \text{ kJ}/\text{kg}$.

Figure 8 illustrates the model with the lighter shade of gray representing the aluminum and the darker gray the silica sand mold. Figure 9 illustrates the model with the same parameters of the previous one with added alumina conductivity represented in black in the corner. The heat flux difference between figure 10 and 11 illustrate that heat can be manipulated, this manipulation results in a more homogenous cooling temperature in figure 11. The heat transfer is lowered in the corner, therefore the calories move faster on the sides.

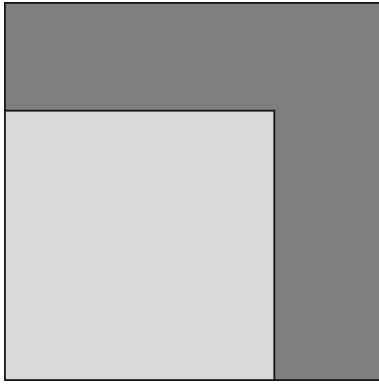


Figure 8 Comsol 2D mono material simulation

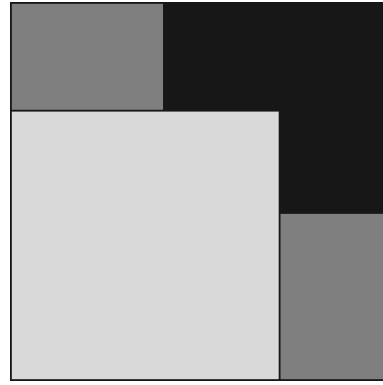


Figure 9 Comsol 2D dual materials simulation

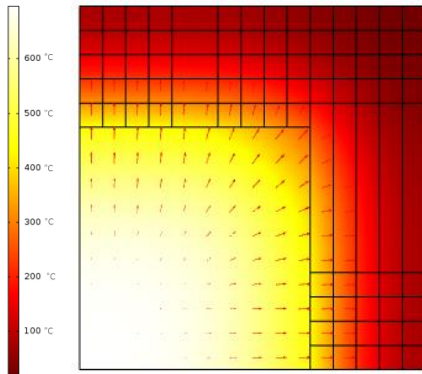


Figure 10 Results of mono material simulation at 0.05 s

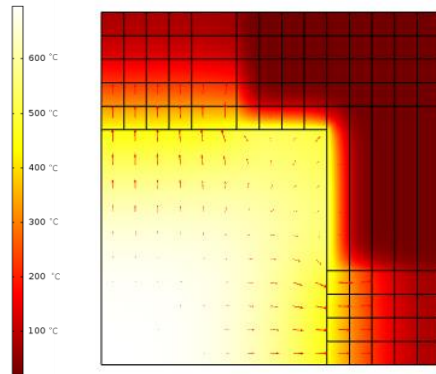


Figure 11 Results of dual material simulation at 0.05 s

The simulation is repeated on a 2D right angle simulation as described by figure 12. It can be noticed on figure 13 and the heat flux stays along the line of the faster cooling speed material. This proposed design is not ideal as it removes calories in the outside corner, which results in a higher thermal gradient resulting in local shrinkage. It is hypothesized at this point that a coupling of faster and slower cooling speed material may further improve casting.

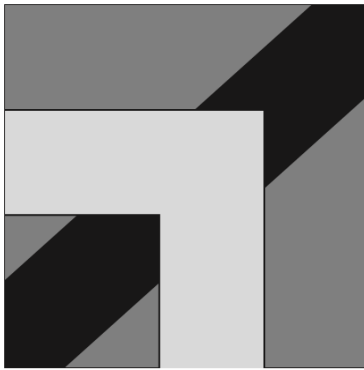


Figure 12 2D Right angle definition

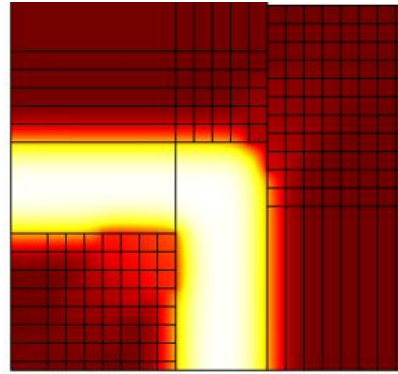


Figure 13 2D Results of right angle simulation

A 3D model is then constructed as to represent better the study case of the cooling of a right angle part as illustrated by figure 14. The rectangle section is 10 mm x 10 mm, with a length of 30 mm and 30 mm. In a later version the inner and outer fillets radius will be of 10 mm. The critical cooling speed section lies on the plan of the inner-outer angle as illustrated by figure 15.

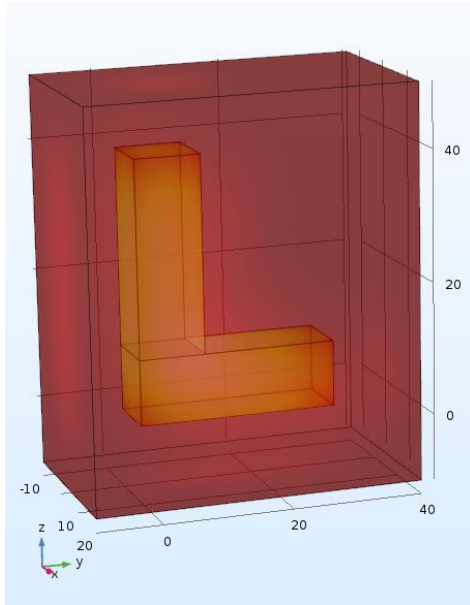


Figure 14 Definition of the right angle

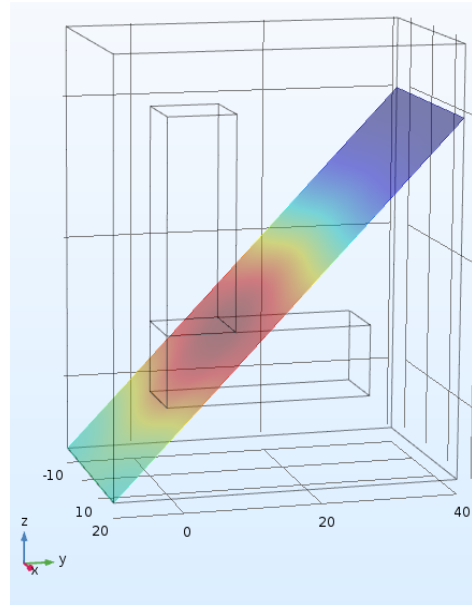


Figure 15 Plan section of interest

3D model simulations were done with ESI ProCAST software as to have a better material behavior during phase change.

Three cases were simulated to compare 1) a conventional design with fillets, 2) a design disrespecting the guideline, 3) and finally the proposed tri material molds. With the goal of having the smallest the thermal gradient possible.

The simulation with the fillets will be the reference guide, figure 16, as it is the recommended configuration. It can be seen on figure 17 that the thermal difference during the mushy zone between point 2 and point 3 is 8 K for a distance of 5.65 mm which results in a 1.4 K/mm gradient, the second highest value during the cooling is 0.9 K/mm at the end of the mushy zone.

The cooling speed on the 613 °C to 570 °C section is 8.6 K/s. Therefore the Niyama criterion is at $0.05 \text{ (K}\cdot\text{s)}^{-1/2}\cdot\text{cm}^{-1}$.

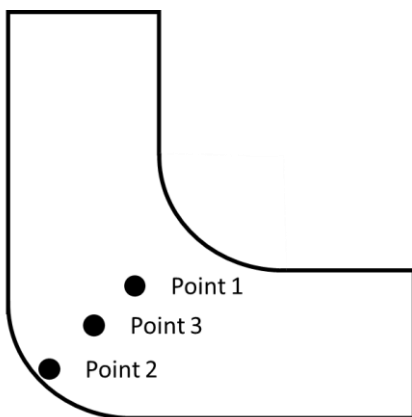


Figure 16 2D section of fillet design

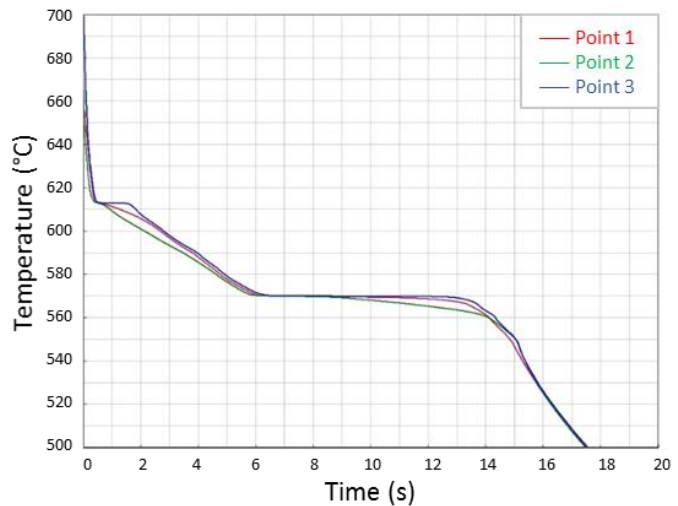


Figure 17 Simulation results of fillet design

The second simulation, figure 18, is what we would like to cast but are told not to as shrinkage occurs. The mold is composed of silica sand. In this simulation the thermal gradient is higher than the reference case with the highest gradient being at 2.1 K/mm and the second highest at 1.45 K/mm, figure 19. The Niyama coefficient is $0.074 \text{ (K}\cdot\text{s)}^{-1/2}\cdot\text{cm}^{-1}$, which is more than the previous simulation and less than the theoretical threshold for shrinkage; implying that this should work.

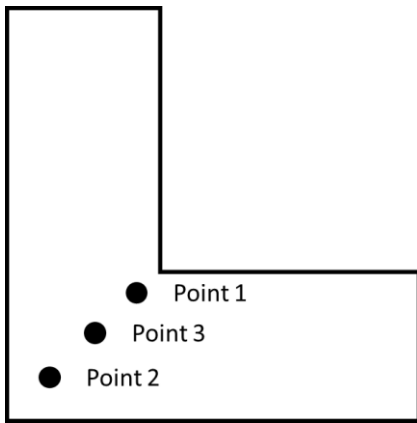


Figure 18 2D section of right angle of mono material

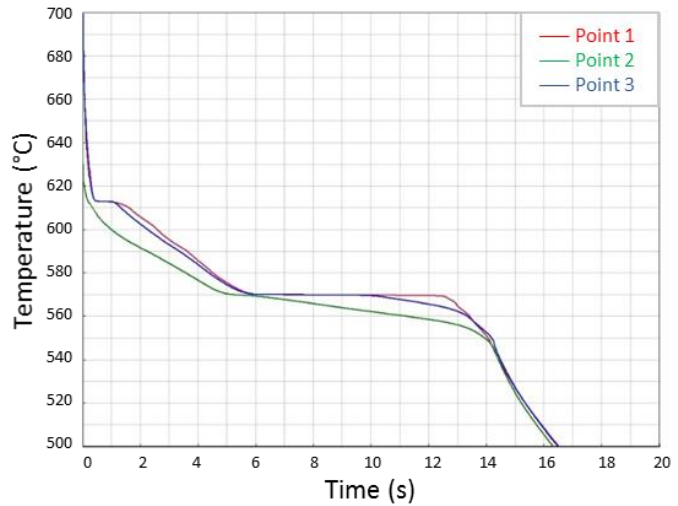


Figure 19 Simulation results of right angle mono material design

The third simulation, figure 20, models a lower than silica sand thermal conductivity at the outer edge and a faster cooling speed than silica sand at the inner corner; the other parts of the mold are modeled with silica sand. The value for lower thermal conductivity is chosen at $0.1 \text{ W}/(\text{m}\cdot\text{K})$, the faster cooling at $10 \text{ W}/(\text{m}\cdot\text{K})$ and regular silica sand at $0.7 \text{ W}/(\text{m}\cdot\text{K})$. The result, figure 21, is encouraging as the curves almost overlay each other, suggesting an even thermal gradient during cooling.

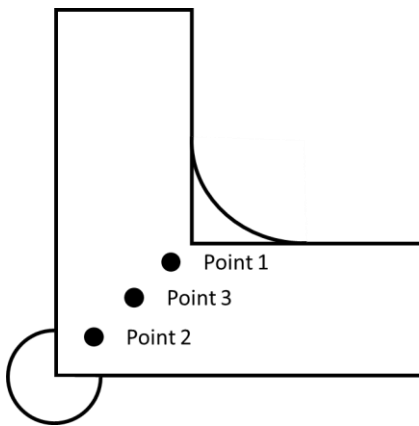


Figure 20 2D section of right angle of trimaterial

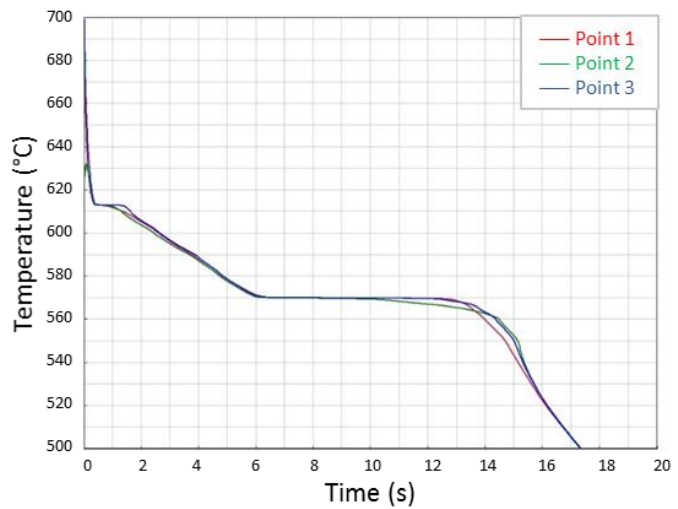


Figure 21 Simulation results of right angle trimaterial design

Finally, a sample representing the third simulation is fabricated with conventional modeler's tools, figure 22. The cutaway allows a better view of the material placement. The different materials were added one after the other during the build process. The alumina based material had difficulties sticking to the silica based sand. This could be because the particles size are not the same but the added binder ratio was the same. Aluminum was not a difficulty to add. The sprue, riser, and runner need to be added before casting this mold.



Figure 22 Cutaway of the trimerial sand mold

4. Conclusion

The proposed methodology of multi material 3D printing for sand casting has potential in reducing hot spots by varying the thermal conductivity. This methodology can also displace hotspots to a more manageable place. Instrumented molds will give more accurate thermal property data. Furthermore, the influence of the mold coating, and the recycling aspect were not taken in to account in this study and should be investigated.

A multiple material printing machine will ease the mold fabrication process as no assembly would be required.

Acknowledgments

The authors would like to thank financial support from l'Agence Nationale de la Recherche (Grant, ANR-15-CE08-0037).

References

- [1] G. Casalino, L. a. C. De Filippis, a. D. Ludovico, and L. Tricarico, "An investigation of rapid prototyping of sand casting molds by selective laser sintering," *Journal of Laser Applications*, vol. 14, no. 2, p. 100, 2002.
- [2] D. King and T. Tansey, "Alternative materials for rapid tooling," vol. 121, no. September 2001, pp. 313–317, 2002.
- [3] Y. Bai and C. B. Williams, "An Exploration of Binder Jetting of Copper," *Rapid Prototyping Journal*, 2015.
- [4] S. M. Gaytan, M. A. Cadena, H. Karim, D. Delfin, Y. Lin, D. Espalin, E. MacDonald, and R. B. Wicker, "Fabrication of barium titanate by binder jetting additive manufacturing technology," *Ceramics International*, vol. 41, no. 5, pp. 6610–6619, 2015.
- [5] K. Myers, P. Cortes, B. Conner, T. Wagner, B. Hetzel, and K. M. Peters, "Structure property relationship of metal matrix syntactic foams manufactured by a binder jet printing process," *Additive Manufacturing*, vol. 5, pp. 54–59, 2015.
- [6] R. Ponche, O. Kerbrat, P. Mognol, and J. Hascoët, "A novel methodology of design for Additive Manufacturing applied to Additive Laser Manufacturing process," *Robotics and Computer-Integrated Manufacturing*, vol. 30, no. 4, pp. 389–398, 2014.
- [7] N. a. Meisel and C. B. Williams, "Design For Additive Manufacturing: An Investigation Of Key Manufacturing Considerations In Multi-Material Polyjet 3d Printing," *Solid Freeform Fabrication Symposium*, pp. 746–763, 2014.
- [8] J. wu Kang and Q. xian Ma, "The role and impact of 3D printing technologies in casting," *China Foundry*, vol. 14, no. 3, pp. 157–168, 2017.

- [9] J. Mun, J. Ju, and J. Thurman, "Indirect Additive Manufacturing of a Cubic Lattice Structure with a Copper Alloy," in *Proceedings of 24th Annual International Solid Freeform Fabrication Symposium*, 2014, pp. 665–687.
- [10] J. Mun, B. G. Yun, J. Ju, and B. M. Chang, "Indirect additive manufacturing based casting of a periodic 3D cellular metal - Flow simulation of molten aluminum alloy," *Journal of Manufacturing Processes*, vol. 17, pp. 28–40, 2015.
- [11] N. a. Meisel, C. B. Williams, and A. Druschitz, "Lightweight Metal Cellular Structures via Indirect 3D Printing and Casting," *Solid Freeform Fabrication Symposium*, pp. 162–176, 2012.
- [12] T. Le Néel, P. Mognol, and J. Y. Hascoët, "Design methodology for variable shell mould thickness and thermal conductivity additively manufactured." International Congress on Welding, Additive Manufacturing and Associated Non Destructive Testing, 2017.
- [13] J. Y. Hascoët, P. Muller, and P. Mognol, "Manufacturing of Complex Parts with Continuous Functionally Graded Materials (FGM)," *Solid Freeform Fabrication Symposium*, pp. 557–569, 2011.
- [14] W. C. Krumbein and L. L. Sloss, "Stratigraphy and sedimentation," *Soil Science*, vol. 71, no. 5, p. 401, 1951.
- [15] E. S. Huetter, N. I. Koemle, G. Kargl, and E. Kaufmann, "Determination of the effective thermal conductivity of granular materials under varying pressure conditions," *Journal of Geophysical Research*, vol. 113, no. E12, p. E12004, 2008.
- [16] S. R. Sama and G. P. Manogharan, "Sand Casting Design Rules," 2017.
- [17] R. Tavakoli, "On the prediction of shrinkage defects by thermal criterion functions," *International Journal of Advanced Manufacturing Technology*, no. September, pp. 0–31, 2014.
- [18] E. Liotti and B. Previtali, "Study of the validity of the Niyama criteria function applied to the alloy AlSi7Mg," *Metallurgia Italiana*, vol. 98, no. 9, pp. 33–37, 2006.